A convolutional neural-network model of human cochlear mechanics and filter tuning for real-time applications

Deepak Baby, Arthur Van Den Broucke, Sarah Verhulst

Hearing Technology @ WAVES, Dept. of Information Technology, Ghent University, 9000 Ghent, Belgium

* s.verhulst@ugent.be; deepakbabycet@gmail.com

Abstract

Auditory models are commonly used as feature extractors for automatic speech-recognition systems or as front-ends for robotics, machine-hearing and hearing-aid applications. Although auditory models can capture the biophysical and nonlinear properties of human hearing in great detail, these biophysical models are computationally expensive and cannot be used in real-time applications. We present a hybrid approach where convolutional neural networks are combined with computational neuroscience to yield a real-time end-to-end model for human cochlear mechanics, including level-dependent filter tuning (CoNNear). The CoNNear model was trained on acoustic speech material and its performance and applicability were evaluated using (unseen) sound stimuli commonly employed in cochlear mechanics research. The CoNNear model accurately simulates human cochlear frequency selectivity and its dependence on sound intensity, an essential quality for robust speech intelligibility at negative speech-to-background-noise ratios. The CoNNear architecture is based on parallel and differentiable computations and has the power to achieve real-time human performance. These unique CoNNear features will enable the next generation of human-like machine-hearing applications.

Introduction

The human cochlea is an active, nonlinear system that transforms sound-induced vibrations of the middle-ear bones to cochlear travelling waves of basilar-membrane (BM) motion [1]. Cochlear mechanics and travelling waves are responsible for hallmark features of mammalian hearing, including the level-dependent frequency selectivity [2–5] that results from a cascade of cochlear mechanical filters with centre frequencies (CFs) between 20 kHz and 40 Hz from the human cochlear base to apex [6].

Modelling cochlear mechanics has been an active field of research because computational methods can help characterise the mechanisms underlying normal or impaired hearing and thereby improve hearing diagnostics [7,8] and treatment [9,10], or inspire machine-hearing applications [11,12]. One popular approach involves representing the cochlea as a transmission line (TL) by discretising the space along the BM and describing each section using a system of ordinary differential equations that approximate the local biophysical filter characteristics (Fig. 1a; state-of-the-art model) [13–19]. Analytical TL models represent the cochlea as a cascaded system in which the response of each section depends on the responses of all previous sections. This architecture makes them computationally expensive, as the filter operations in the different sections cannot be computed in parallel. The computational complexity is even greater when nonlinearities or feedback pathways are included to faithfully approximate cochlear mechanics [15,20].

Computational complexity is the main reason that real-time applications for hearing-aid [21], robotics [22], and automatic speech recognition applications do not adopt cochlear travelling-wave models in their preprocessing. Instead, they use computationally efficient approximations of auditory filtering that compromise on key auditory features. A common simplification implements the cochlear filters as a parallel, rather than cascaded, filterbank [23, 24]. However, this parallel architecture captures neither the longitudinal coupling

properties of the BM [25] nor the generation of otoacoustic emissions [26]. Another popular model, the gammatone filterbank model [27], ignores the stimulus-level dependence of cochlear filtering. Lastly, a number of models simulate the level-dependence of cochlear filtering but fail to match the performance of TL models [28]: they either simulate the longitudinal cochlear coupling locally within the individual filters of the uncoupled filterbank [29] or introduce distortion artefacts when combining an automatic-gain-control type of level-dependence with cascaded digital filters [30–32].

Thus, the computational complexity of biophysically realistic cochlear models poses a serious impediment to the development of human-like machine-hearing applications. This complexity motivated our search for an efficient model that matches the performance of state-of-the-art analytical TL models while offering real-time execution. Here, we investigate whether convolutional neural networks (CNNs) can be used for this purpose. Neural networks of this type can deliver end-to-end waveform predictions [33, 34] with real-time properties [35] and are based on convolutions akin to the filtering process associated with cochlear processing.

This paper details how CNNs can best be connected and trained to approximate the computations performed by TL cochlear models [19, 36, 37], with a specific emphasis on simultaneously capturing the tuning, level-dependence, and longitudinal coupling characteristics of human cochlear processing. The proposed model (*CoNNear*) converts speech stimuli into corresponding BM displacements across 201 cochlear filters distributed along the length of the BM. Unlike TL models, the CoNNear architecture is based on parallel CPU computations that can be accelerated through GPU computing. Consequently, CoNNear can easily be integrated with real-time auditory applications that use deep learning. The quality of the CoNNear predictions and the generalisability of the method are evaluated on the basis of cochlear mechanical properties such as filter tuning estimates [38], nonlinear distortion characteristics [39], and spatial excitation patterns [40] obtained using sound stimuli commonly adopted in experimental studies of cochlear mechanics but not included in the training.

The CoNNear model

The CoNNear model has an auto-encoder CNN architecture and transforms a 20-kHz sampled acoustic waveform (in [Pa]) to N_{CF} cochlear BM displacement waveforms (in [μm]) using several CNN layers and dimension changes (Fig. 1a). The first four layers are *encoder* layers and use strided convolutions, to halve the temporal dimension after every CNN layer. The following four, *decoder*, layers map the condensed representation onto $L \times N_{CF}$ outputs using deconvolution operations. L corresponds to the initial size of the audio input and N_{CF} to 201 cochlear filters with centre frequencies (CFs) between 0.1 and 12 kHz. The adopted CFs were spaced according to the Greenwood place-frequency map of the cochlea [6] and span the most sensitive frequency range of human hearing [41]. It is important to preserve the temporal alignment (or, phase) of the inputs across the architecture, because this information is essential for speech perception [42]. We used U-shaped skip connections for this purpose. Skip connections have earlier been adopted in image-to-image translation [43] and speech-enhancement applications [33, 34]; they pass temporal information directly from encoder to decoder layers (Fig. 1a; dashed arrows). Aside from preserving phase information across the architecture, skip connections may improve the model's ability to learn how best to combine the nonlinearities of several CNN layers to simulate the level-dependent properties of human cochlear processing.

Every CNN layer is comprised of a set of filterbanks followed by a nonlinear operation [44] and the CNN filter weights were trained using TL-simulated BM displacements from N_{CF} cochlear channels [37]. While training was conducted using a speech corpus [45] presented at 70 dB SPL, model evaluation was based on the ability to reproduce key cochlear mechanical properties using basic acoustic stimuli (e.g. clicks, pure-tones) unseen during training (Fig. 1c). During training and evaluation, the audio input was segmented into 2048-sample windows ($\approx$100 ms), after which the corresponding BM displacements were simulated and concatenated over time. Because CoNNear treats each input independently, and resets its adaptation properties at the start of each simulation, this concatenation procedure could result in discontinuities near the window boundaries. To address this issue, we also evaluated an architecture that had the previous and
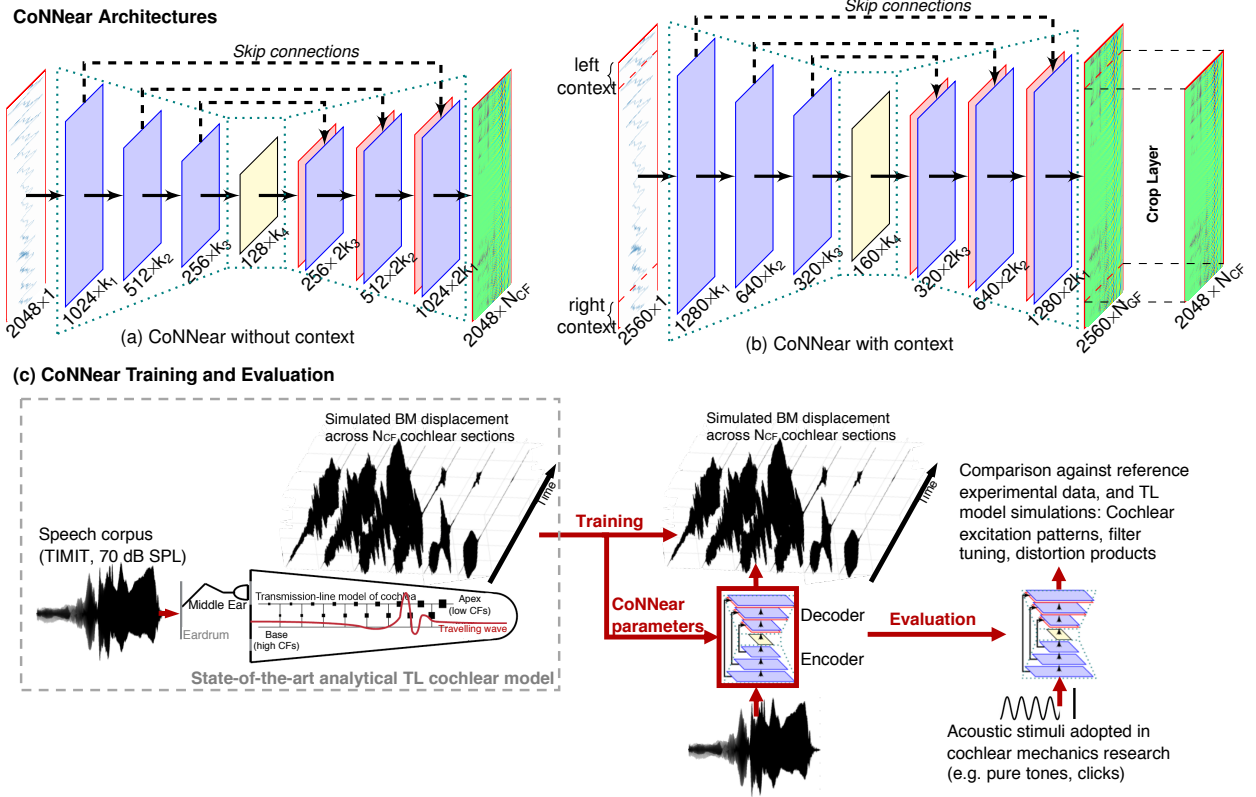
CoNNear Architectures

(a) CoNNear without context

(b) CoNNear with context

(c) CoNNear Training and Evaluation

Fig 1. CoNNear Overview. CoNNear is a fully convolutional encoder-decoder neural network with strided convolutions and skip-connections to map audio input to 201 basilar-membrane vibration outputs of different cochlear sections (N_{CF}) in the time-domain. CoNNear architectures with (a) and without (b) context are shown. The final CoNNear model has four encoder and decoder layers, uses context and includes a tanh activation function between the CNN layers. (c) provides an overview of the model training and evaluation procedure. Whereas reference, analytical TL-model simulations to a speech corpus were used to train the CoNNear parameters, evaluation of the model was performed using simple acoustic stimuli commonly adopted in cochlear mechanics studies.

following (256) input samples available as context (Fig. 1b). Different from the no-context architecture (Fig. 1a), a final cropping layer was added to remove the simulated context and yield the final L-sized BM displacement waveforms. Additional details on the CoNNear architecture and training procedure are given in Methods and Extended Data Table 1. Lastly, thanks to its convolutional architecture, training CoNNear using audio inputs of fixed duration does not prevent it from handling inputs of other durations after training. This flexibility is a clear benefit over matrix-multiplication-based neural network architectures, which can operate only on inputs of fixed-duration.

CoNNear hyperparameter tuning

Critical to this work is proper determination of the optimal CNN architecture and its hyperparameters that yield a realistic model for cochlear processing. Ideally, CoNNear should both simulate the speech training dataset with a sufficiently low L1 loss [i.e., the average mean-absolute difference between simulated BM displacements of the reference TL and CoNNear model] and also reproduce key cochlear response properties. The hyperparameters that can be adjusted to define the final CoNNear architecture are given in Extended Data Table 1. To determine the hyperparameters (number of layers, nonlinearity, context), we followed an iterative principled approach taking into account: (i) the L1 loss on speech material, (ii) the desired

frequency- and level-dependent cochlear filter tuning characteristics, and (iii), the computational load needed for real-time execution. Afterwards, the prediction accuracy of CoNNear was evaluated on a broader set of response features. We considered a total of four metrics based on cochlear responses evoked using simple stimuli of different frequencies and levels: filter tuning (Q_{ERB}), click-evoked dispersion, pure-tone excitation patterns, and the generation of cochlear distortion products. Together, these evaluation metrics form a comprehensive description of cochlear processing. Further information on the tests and their implementation is given in Methods. A benefit of our approach is that the evaluation stimuli were *unseen* to the model to ensure an independent evaluation procedure. Even though any fragment of the speech training material can be seen as a combination of basic acoustic elements such as impulses and pure tones of varying levels and frequencies, the cochlear mechanics stimuli were not explicitly present in the training material.

The first hyperparameter specifies the total number of encoder/decoder layers, which we set to 8 on the basis of Q_{ERB} simulations. Aside from the reference experimental human Q_{ERB} curve for low stimulus levels [46], Fig. 2a shows simulated Q_{ERB} curves from the reference TL-model (red) overlaid with CoNNear-model simulations. CoNNear captures the frequency-dependence of the human and reference TL Q_{ERB} function better as the layer depth was increased from 4 to 8. Models with 4 and 6 layers underestimated the overall Q_{ERB} function and performed worse for CFs below 1 kHz where reference ERBs were narrower, and corresponding BM impulse responses longer, than for higher CFs. Extending the number of layers beyond 8 increased the required computational resources without producing a substantial improvement in the quality of the fits. These resources are listed in Extended Data Table 2 for models of different layers, along with L1-loss predictions on the speech training set and a small set of evaluation metrics.

The second hyperparameter controls the activation function, or nonlinearity, which is placed between the CNN layers. To mimic the original shape of the outer-hair-cell input/output function [47] responsible for cochlear compression, we required that the activation function cross the x-axis; we therefore considered only the parametric rectified linear unit (PReLU) and hyperbolic-tangent (tanh) nonlinearities rather than standard activation functions such as the sigmoid and ReLU. Figure 2b depicts how the PreLU and tanh activation functions affected the simulated Q_{ERB}s across CFs. Whereas the PReLU activation function was unable to capture the level-dependence of cochlear filter tuning, the tanh nonlinearity reproduced both the level and frequency-dependence of human Q_{ERB}s. Additionally, Extended Data Table 3 (no context simulations) shows that the model with tanh nonlinearity reached a lower L1 loss on both training and test sets compared to the PReLU nonlinearity, while requiring a smaller number of parameters. The benefit of the tanh nonlinearity is further illustrated when comparing simulated pure-tone excitation patterns across model architectures. Figure 3 shows that the tanh nonlinearity (c) outperforms the PReLU nonlinearity (b) in capturing the compressive growth of BM displacement with stimulus level, as observed in the excitation pattern maxima (a). Although both activation functions were able to code negative input deflections, only the model with tanh nonlinearity (whose shape best resembles the cochlear input/output function) performed well. These simulations show that it is essential to consider the shape of the activation function when the reference system is nonlinear.

The final hyperparameter relates to adding context information when simulating an input of size L. As noted earlier, CNN architectures treat each input independently, which can produce discontinuities near the window boundaries. The effect of adding context [cf. architecture (b) vs (a) in Fig. 1] is best observed when simulating speech. Figure 4 shows simulated BM displacements of the reference and CoNNear models to a segment of the speech test set which was not seen during training. Panel (d) shows that providing context prevents discontinuities near the window boundaries. Context was also beneficial when simulating the reference 70-dB Q_{ERB} function in Fig. 2c. The L1-loss simulations in Extended Data Table 3 (tanh simulations) confirmed the overall performance improvement when providing context, and hence the final CoNNear architecture included a context window of 256 samples on either side of the 2048 sample input (Fig. 1b).
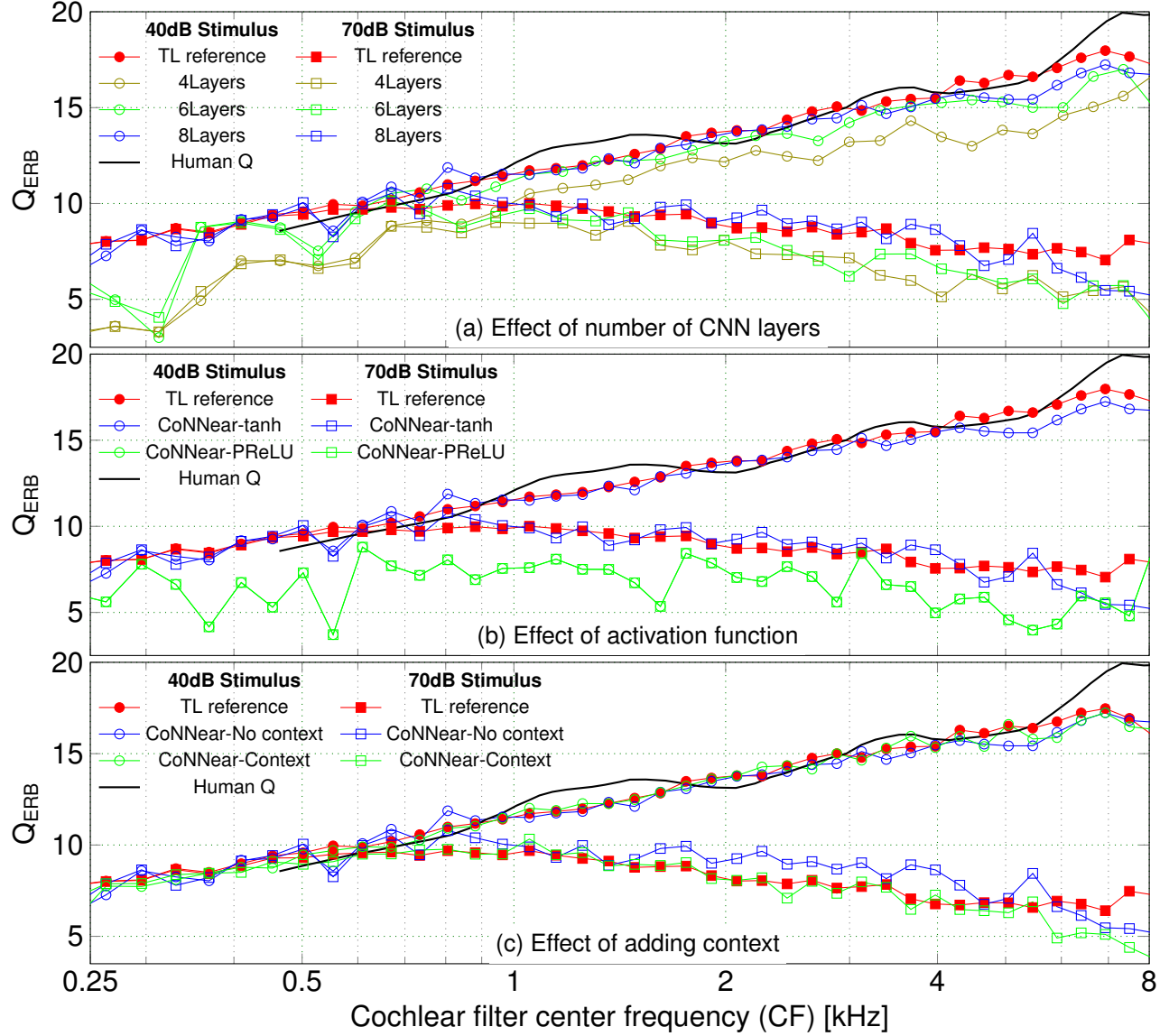
Fig 2. CoNNear hyperparameter tuning. Cochlear filter tuning (Q_{ERB}) was simulated to 100-μs clicks of 40 and 70 dB peSPL for different cochlear filter centre frequencies (CF). Reference human Q_{ERB} estimates for low-stimulus levels [46] are shown and compared to simulations of the reference TL model and CoNNear models with (c) and without (a,b) context. (a) Increasing the number of CoNNear layers from 4 to 8, improved the Q_{ERB}-across-CF simulations. (b) Comparing architectures with the PReLU or tanh activation function shows that the PReLU nonlinearity failed to capture level-dependent cochlear filter tuning because the Q_{ERB} functions remained invariant to stimulus level changes. 8-layer CNN architectures were used for this simulation. (c) Adding context to the 8-layer, tanh model further improved the CoNNear predictions by showing less Q_{ERB} fluctuations across CF.

Generalisability of CoNNear

Overfitting occurs when the trained model merely memorises the training material and fails to generalise to data not present in the training set. To investigate whether the final CoNNear architecture was robust against overfitting, we tested how well the trained CoNNear model performed on unseen stimuli from (i) the same database, (ii) a different database of the same language, (iii) a different database of a different language, and (iv) a music piece.
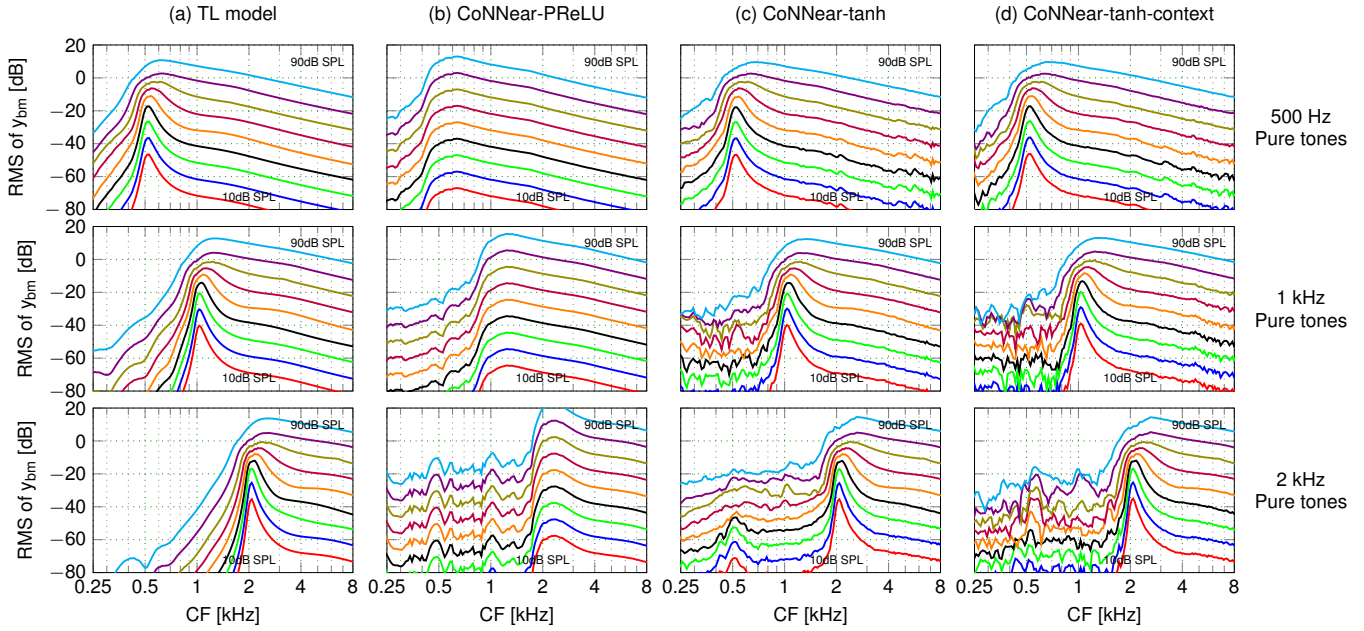
Fig 3. Comparing cochlear excitation patterns across model architectures. Simulated root-mean-square (RMS) levels of BM displacement across CF for pure-tone stimuli between 10 and 90 dB SPL. From top to bottom, the stimulus frequencies were 500 Hz, 1 kHz and 2 kHz, respectively. Both the reference, TL-model, level-dependent excitation pattern shape changes and compressive growth of pattern maxima (a), were captured by the tanh architectures (c,d), but not by the PReLU architecture (b).

Figure 5 shows a boxplot of the distribution of L1 losses calculated for each of the simulated windows of the TIMIT training material (a), for the TIMIT test set using different speakers (b), and for the Dutch Matrix sentence database [48] (c). In addition to calculated loss distributions, Fig. 6 compares instantaneous BM displacement intensities between the reference TL-model (b) and CoNNear (c) for three stimuli unseen during training: (i) an English sentence from the Wall Street Journal Corpus [49] to show how CoNNear adapts to different recording settings (first column). (ii) a sentence from the Dutch matrix test [48] to investigate performance on a different language stimulus (middle column), and (iii) a music segment to test performance on a non-speech acoustic stimulus (right column). From an application perspective, we also tested how CoNNear handles audio input of arbitrary length. Extended Data Figure 1 shows that CoNNear generalises well to an unseen speech stimulus of length 0.5 s (10048 samples) and a music stimulus of length 0.8 s (16384 samples), even though training was performed using shorter windows of fixed duration (2048 samples). The similar loss distribution functions across test conditions in Fig. 5, together with the small intensity prediction errors seen in Fig. 6d, show that CoNNear generalises well to unfamiliar stimuli.

CoNNear as a model for human cochlear signal processing

Since the primary goal of this work was to develop a neural-network based model for human cochlear mechanics, we evaluated how well the trained CoNNear model collectively performs on simulating key cochlear mechanics metrics (see Methods for a detailed description). Figure 2c shows that the final CoNNear architecture with context simulates the frequency- and level-dependence of human cochlear tuning. At the same time, CoNNear faithfully captures the shape and compression properties of pure-tone cochlear excitation patterns (Fig. 3d). However, we did observe small excitation pattern fluctuations at CFs below the stimulus frequency for the 1 and 2 kHz simulations (middle and bottom row in Fig. 3). These fluctuations had levels of approximately 30 dB below the peak of the excitation pattern and are not expected to degrade the sound-driven response of CoNNear to complex stimuli such as speech. This latter statement is supported
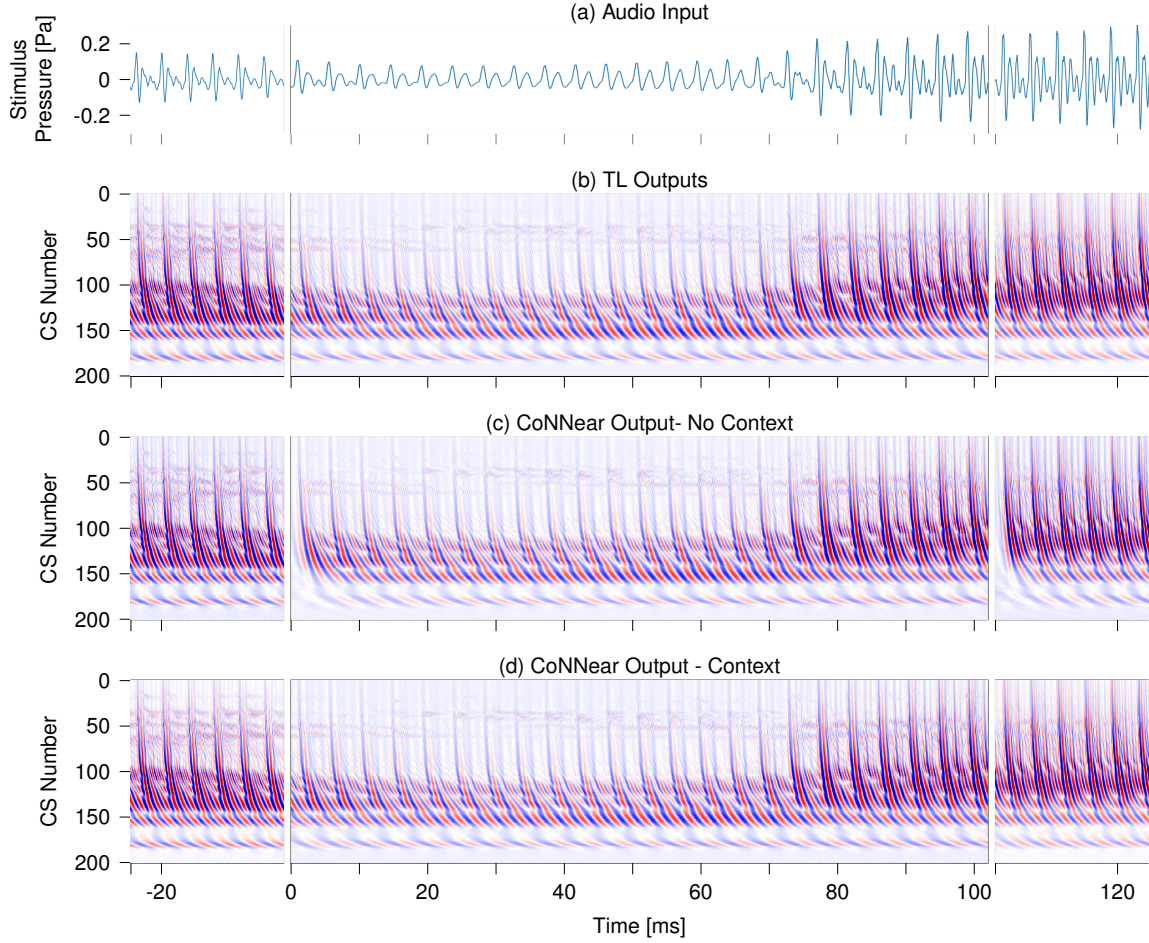
6

Fig 4. Effect of adding context to the CoNNear simulations. Simulated BM displacements for a 2048-sample-long speech fragment of the TIMIT test set (i.e., unseen during training). The stimulus waveform is shown in panel (a) and panels (b)-(d) depict instantaneous BM displacement intensities (darker colours = higher intensities) of simulated TL-model outputs (b) and two CoNNear architecture outputs: without (c) and with (d) context. The left and right segments show the output of the neighbouring windows to demonstrate the discontinuity over the boundaries. The N_{CF}=201 output channels are labelled per channel number: channel 1 corresponds to a CF of 12 kHz and channel 201 to a CF of 100 Hz. Intensities varied between -0.5 μm (blue) and 0.5 μm (red) for all panels.

both by the CoNNear speech simulations in Fig. 4, which show no visible noise in the error patterns, and by computing the root mean-square error (RMSE) between simulated TL and CoNNear model excitation patterns for a broad range of frequencies and levels (Extended Data Fig.2c). To obtain a meaningful error estimate, we normalised the RMSE to the TL excitation pattern maximum to yield a CoNNear error percentage. The error for the final CoNNear architecture remained below 5 % for pure-tone frequencies up to 4 kHz, and stimulation levels below 80 dB, but increased both for higher stimulus levels and at CFs of 8 and 10 kHz. The larger error percentages result from the overall level and frequency content of the speech material used for training. The dominant energy in speech occurs below 5 kHz, and we presented the speech corpus at 70 dB. However, it is noteworthy that the visual difference between simulated high-level excitation patterns was mostly associated with low-level fluctuations at CFs below the stimulation frequency and not at the stimulation frequency itself (cf. the first and last columns of Fig. 3). This means that the stimulus-driven error that occurs when using broadband stimuli is likely smaller than that observed here for tonal stimuli. In summary, the error appears acceptable for processing speech-like audio. We speculate that its application range can be extended by retraining with stimuli at different levels and/or with greater
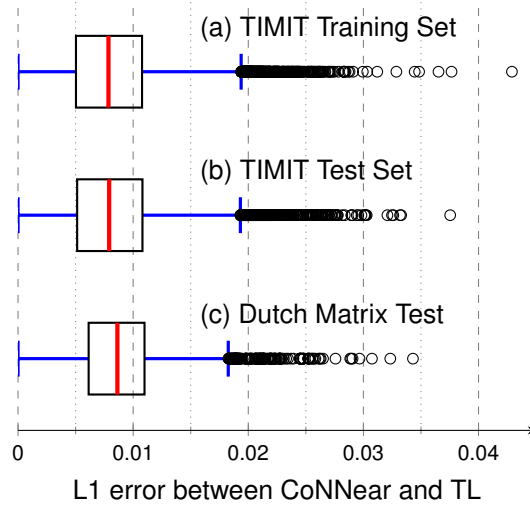
Fig 5. Boxplots comparing the distribution of L1 losses between TL-model and CoNNear model simulations. L1 errors were computed for all simulated windows of length 2048 within (a) 2310 sentences from the TIMIT training set (131760 simulated L1 losses) (b) the TIMIT test set containing 550 sentences (32834 simulated L1 losses) and (c) 100 sentences from the Dutch Matrix test (7903 simulated L1 losses). The red line in the boxplot shows the median of the L1 errors, the black box denotes the values between the 25% (Q1) and 75% (Q3) quartiles. The blue whiskers denote the error values that fall within the 1.5 * (Q3 - Q1) range. Outliers are shown as circles. Cochlear model predictions and prediction errors for the epochs associated with the median and maximum L1 loss are shown in Extended Data Fig. 3.

high-frequency content.

Figure 7 shows the dispersion characteristics of the TL model and trained CoNNear models, illustrating the characteristic 12-ms onset delay from basal (high CF, low channel numbers) to apical (low CF, high channel numbers) cochlear sections in both models. In the cochlea, dispersion arises from the biophysical properties of the coupled BM (i.e., its spatial variation of stiffness and damping), and the CoNNear architecture captures this phenomenon. Adding context did not affect the simulation quality.

Finally, we tested CoNNear's ability to simulate a last, key feature of cochlear mechanics: distortion products, which travel in reverse along the BM to generate pressure waveforms in the ear canal (i.e., distortion product otoacoustic emissions, DPOAEs). Figure 8 compares reference TL-model simulations with those of different CoNNear models (b)-(d). DPOAE frequencies are visible as spectral components not present in the stimulus (which consists of two pure tones at frequencies $f_1 = 2.0$ kHz and $f_2 = 2.4$ kHz). In humans, the strongest DP component occurs at $2f_1 - f_2 = 1.6$ kHz, and as the simulations show, the level of this DP was best captured using the tanh activation function. As observed before in the excitation pattern simulations, the activation function most resembling the shape of the cochlear nonlinearity performed best when simulating responses that rely on cochlear compression. Adding context removed the high-frequency distortions that were visible in panels (b) and (c).

The quality of the DPOAE simulations across a range of stimulation levels and frequencies was further investigated in Fig. 8e. Up to L_2 levels of 60 dB SPL, CoNNear matched the characteristic nonlinear growth of both TL-simulated and human DPOAE level functions well [51]. At higher stimulation levels, DPOAE levels started fluctuating in both models. Although this may reflect the chaotic character of cochlear DPs interacting with cochlear irregularities in TL models and in human hearing [26], it may simply reflect the limited training material we had available for CoNNear at these higher levels. Given that human DPOAEs are generally recorded for stimulation levels below 60 dB SPL in clinical or research contexts [52], we can conclude that CoNNear was able to capture this important epiphenomenon of hearing. The cochlear mechanics evaluations we performed in Figs. 2, 7, 3, 8 and Extended Data Fig.2 together demonstrate that the 8-layer, tanh, CoNNear model with context performed best on four crucial aspects of human cochlear
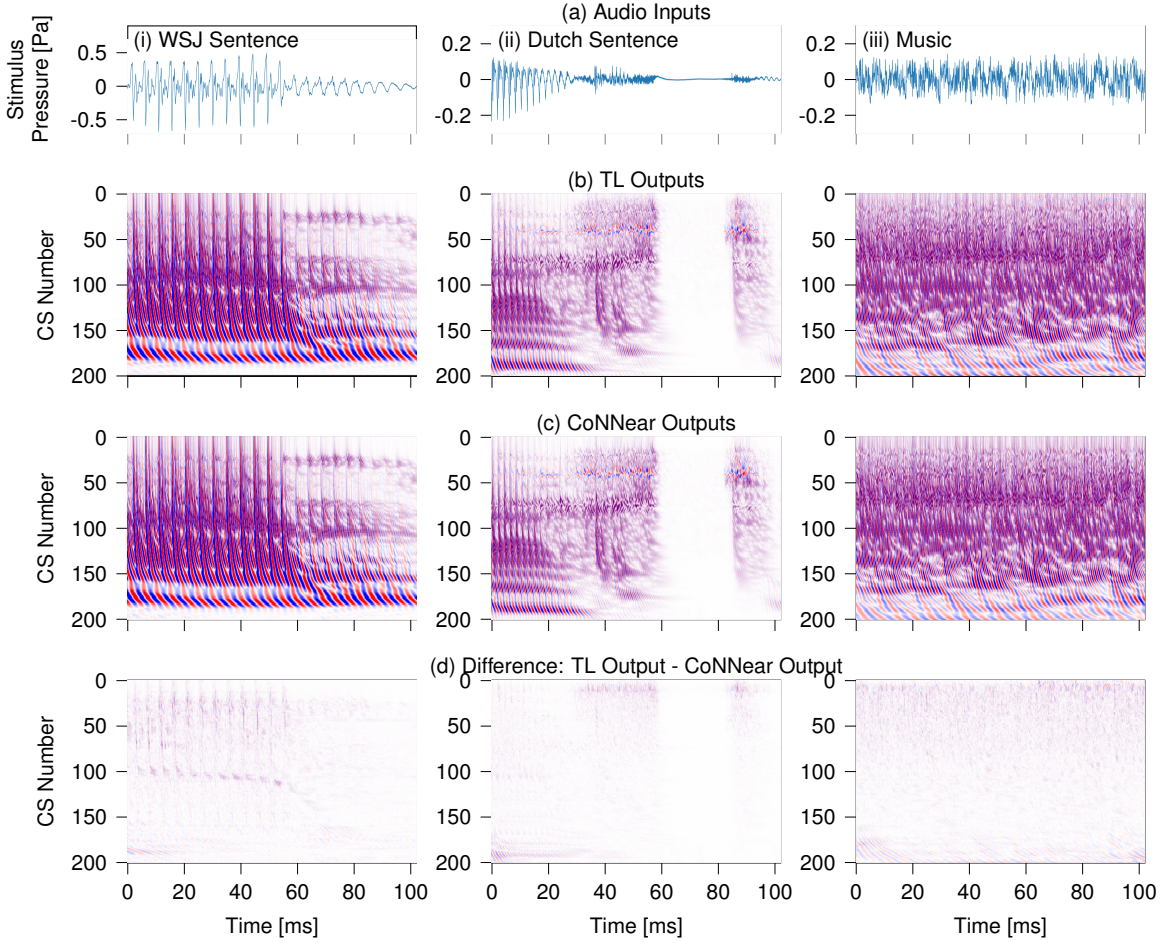
8

Fig 6. Evaluating how well CoNNear generalises to unseen audio input. Along the columns, simulated BM displacements for three different audio stimuli of 2048 samples are shown: (i) a recording of the English Wall Street Journal speech corpus [49], (ii) a sentence from the Dutch matrix test [48] and (iii) a music fragment taken from Interpol - Evil. Stimulus waveforms are depicted in panel (a) and panels (b-c) depict instantaneous BM displacement intensities (darker colours = higher intensities) of the simulated TL-model outputs (b) and the CoNNear outputs (c). Panel (d) shows the intensity difference between the TL and CoNNear outputs. The N_{CF}=201 considered output channels are labelled per channel number: channel 1 corresponds to a CF of 12 kHz and channel 201 to a CF of 100 Hz. The same colour map was used for all figures and ranged between -0.5 μm (blue) and 0.5 μm (red).

mechanics. Despite training on a limited speech corpus presented at 70 dB SPL, CoNNear learned to simulate outputs which matched those of biophysically-realistic analytical models of human cochlear processing across level and frequency.

CoNNear as a real-time model for audio applications

In addition to its ability to simulate realistic cochlear mechanical responses, CoNNear operates in real-time. In audio applications, real-time is commonly defined as a computation duration less than 10 ms; below this limit no delay is perceived). Table 1 summarises the necessary time to compute the final CoNNear-context model for a stimulus window of 1048 samples on CPU or GPU architectures. On a CPU, the CoNNear model outperforms the TL-model by a factor of 129 and on a GPU, CoNNear is 2142 times faster. Additionally, the GPU computations show that the trained CoNNear model (8-layers, tanh, with context) has a latency of 7.27 ms, and hence reaches real-time audio processing performance.
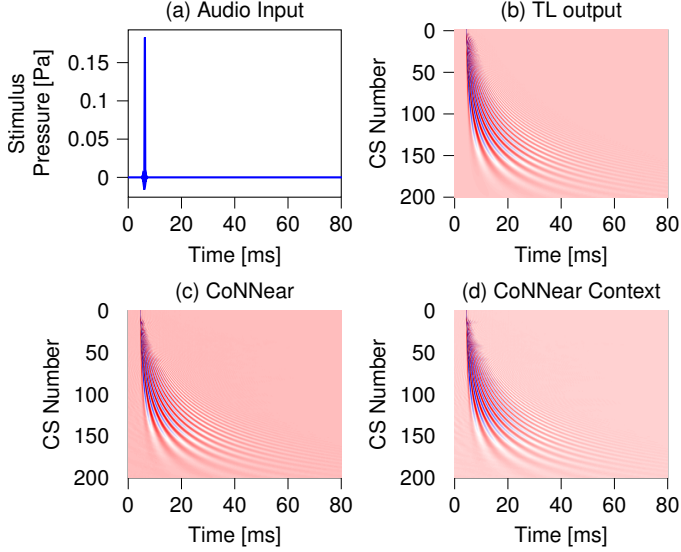
Fig 7. Comparing cochlear dispersion properties across model architectures. Panel (a) shows the stimulus pressure, while panels (b)-(d) show instantaneous BM displacement intensities for CFs (channel numbers, CS) between 100 Hz (channel 201) and 12 kHz (channel 1). The colour scale is the same in all figure panels, and ranges between -15 μm (blue) and 15 μm (red).
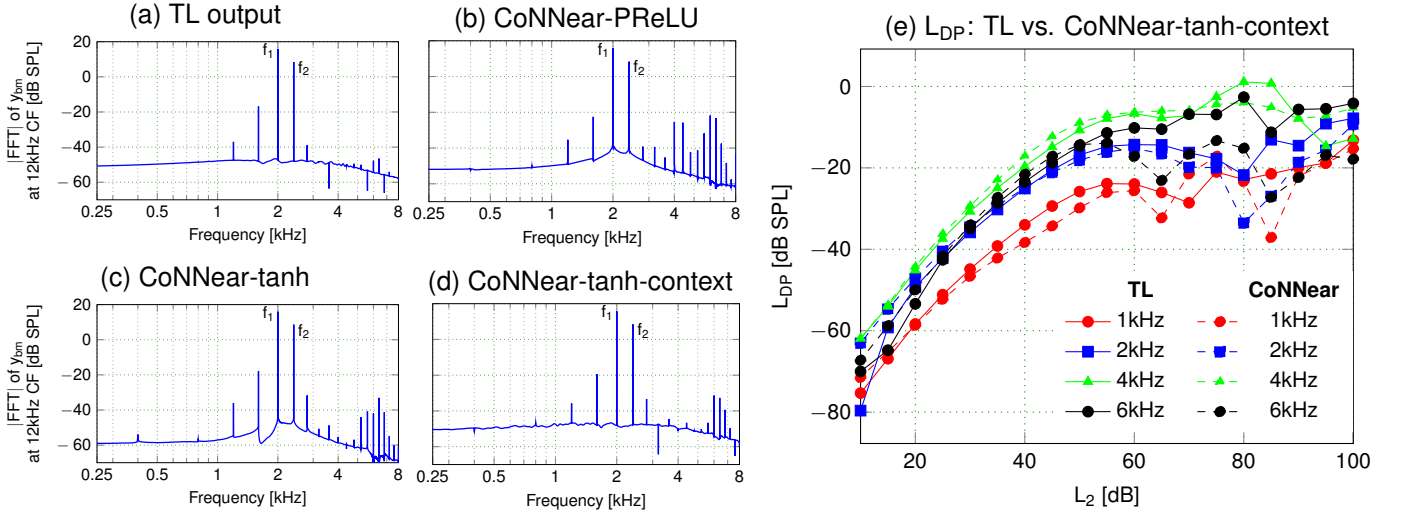

Fig 8. Comparing simulated DPOAEs across model architectures. The frequency response of the 12-kHz CF channel (i.e., fast Fourier transform of the BM displacement waveform) was considered as a proxy for otoacoustic emissions recorded in the ear-canal. In panels (a) - (d), different model simulations are shown in response to two pure tones of f_1 of 2.0 and f_2 of 2.4 kHz. In humans, the most pronounced distortion product occurs at $2f_1 - f_2$ (1.6 kHz). Panel (e) depicts simulated distortion-product levels (L_{DP}) compared between TL and the CoNNear-tanh-context model. L_{DP} was extracted from the frequency response of the 12-kHz CF channel at $2f_1 - f_2$. Simulations were conducted for L_2 levels between 10 and 100 dB SPL and L_1=0.4 L_2+39 [50]. f_1 ranged between 1 and 6 kHz, following an f_2/f_1 ratio of 1.2.

Discussion

This paper details how a hybrid, deep-neural-net and analytical approach can be used to develop a real-time model of human cochlear processing (CoNNear), with performance matching that of human cochlear processing. As we demonstrate here for the first time, neither real-time performance nor biophysically realistic responses need be compromised. CoNNear combines both in a single auditory model, laying the groundwork

Table 1. Model calculation speed. Comparison of the time required to calculate a TL and CoNNear model window of 1048 samples on a CPU (Apple MacBook Air, 1.8 GHz Dual-Core processor) and a GPU (NVIDIA GTX1080). The calculation time for the first window is considered separately for the GPU computations since this window also includes the weight initialisation. For each evaluated category, the best performing architecture is highlighted with a bold font.

Model	#Param	CPU (s/window)	GPU 1st window (s)	GPU (ms/window)
PReLU/8 lay./no context	11,982,464	0.222	1.432	7.70
tanh/8 lay./no context	11,507,328	**0.195**	1.390	7.59
tanh/8 lay./context	11,689,984	0.236	**1.257**	**7.27**
Transmission Line	N/A	25.16	N/A	16918

for a new generation of human-like robotic, speech-recognition and machine hearing applications. Prior work has demonstrated the clear benefits of using biophysically realistic cochlear models as front-ends for auditory applications: e.g. for capturing cochlear compression, [7, 11, 28], speech enhancement at negative signal-to-noise ratio's [12], realistic sound perception predictions [53] and for simulating the generation of human auditory brainstem responses [37, 54]. Hence, CoNNear can dramatically improve performance in application areas which, to date, have relied on computationally intensive biophysical models. Not only can CoNNear operate on running audio input with a latency below 7.5 ms, the model offers a differentiable solution which can be used in closed-loop systems for auditory feature enhancement or augmented hearing.

With the rise of neural-network (NN) based methods, computational neuroscience has seen an opportunity to map audio or auditory brain signals directly to sound perception [55–57] and to develop computationally efficient methods to compute large-scale differential-equation-based neuronal networks [58]. These developments are transformative, as they can unravel the functional role of hard-to-probe brain areas in perception and yield computationally fast neuromorphic applications. The key to these breakthroughs is the hybrid approach in which knowledge from neuroscience is combined with that of NN-architectures [59]. While the possibilities of NN approaches are numerous when large amounts of training data are available, this is rarely the case for biological systems and human-extracted data. It therefore remains challenging to develop models of biophysical systems which can generalise to a broad range of unseen conditions or stimuli.

Our work presents a solution to this problem for cochlear processing by constraining the CoNNear architecture and its hyperparameters on the basis of a state-of-the-art TL cochlear model. Our general approach consists of four steps: First, derive an analytical description of the biophysical system on the basis of available experimental data. Second, use the analytical model to generate a training data set consisting of responses to a representative range of relevant stimuli. Third, use this training data set to determine the NN-model architecture and constrain its hyperparameters. Finally, verify the ability of the model to generalise to unseen inputs. Here, we demonstrated that CoNNear predictions generalise to a diverse set of audio stimuli by faithfully predicting key cochlear mechanics features to sounds which were excluded from the training.

Our proposed method is by no means limited to NN-based models of cochlear processing. Indeed, the method can be widely applied to other nonlinear and/or coupled biophysical models of sensory and biophysical systems. Over the years, analytical descriptions of cochlear processing have evolved based on the available experimental data from human and animal cochleae, and they will continue to improve. It is straightforward to train CoNNear to an updated/improved analytical model in step (i), as well as to include different or additional training data in (ii) to further optimise its performance.

Conclusion

We present a hybrid method which uniquely combines expert knowledge from the fields of computational auditory neuroscience and machine-learning-based audio processing to develop a CoNNear model of human cochlear processing. CoNNear presents an architecture with differentiable equations and operates in real time (< 7.5 ms delay) at speeds 2000 times faster than state-of-the-art biophysically realistic models. We have high hopes that the CoNNear framework will inspire a new generation of human-like machine hearing, augmented hearing and automatic speech-recognition systems.

Methods

Extended Data Table 1 describes the parameters which define the CNN-based CoNNear auto-encoder architecture. The encoder layers transform audio input of size L into a condensed representation of size $L/2^M \times k_M$, where k_M equals the number of filters in the Mth CNN layer. We used 128 filters per layer with a filter length of 64 samples. The encoder layers use strided convolutions, i.e. the filters were shifted by a time-step of two to halve the temporal dimension after every CNN layer. The decoder contains M deconvolution layers to re-obtain the original temporal dimension of the audio input (L). The first three decoder layers used 128 filters per layer and the final decoder layer had (N_{CF}) filters, equalling the number of cochlear sections simulated in the reference cochlear TL model.

Training CoNNear

CoNNear was trained using TL-model simulations of N_{CF} BM displacement waveforms in response to audio input windows of $L = 2048$ samples. For the context architecture (Fig. 1b), the previous and following $L_l = L_r = 256$ input samples were also available to CoNNear. This architecture included a final cropping layer to remove the context after the last CNN decoder and yield an output size $L \times N_{\text{CF}}$. Note that the CoNNear model output units are BM displacement y_{BM} in [μm], whereas the TL-model outputs are in [m]. This scaling was necessary to enforce a training procedure with sufficiently high digital numbers. For training purposes, and visual comparison between the TL and CoNNear outputs, the y_{BM} values of the TL model were multiplied by a factor of 10^6 in all figures and analyses.

    The TIMIT speech corpus [45] was used for training and contains phonetically balanced sentences with sufficient acoustic diversity. To generate the training data, 2310 sentences from the TIMIT corpus were used. They were upsampled to 100 kHz to solve the TL-model accurately [36] and the root-mean square (RMS) energy of every utterance was adjusted to 70 dB sound pressure level (SPL). 550 sentences of the TIMIT dataset were omitted from the training and considered as the test set. BM displacements were simulated for 1000 cochlear sections with centre frequencies between 25 Hz and 20 kHz using a nonlinear time-domain TL model of the cochlea [37]. From the TL-model output representation (i.e., 1000 y_{BM} waveforms sampled at 20 kHz), outputs from 201 CFs between 100 Hz and 12 kHz, spaced according to the Greenwood map [6], were chosen to train CoNNear. Above 12 kHz, human hearing sensitivity becomes very poor [41], motivating our choice for the upper limit of considered CFs. CoNNear model parameters were optimised to minimise the mean absolute error (dubbed L1 loss) between the predicted model outputs and the reference TL model outputs. A learning rate of 0.0001 was used with Adam optimiser [60] and the entire framework was developed using the Keras machine learning library [61] with a Tensorflow [62] back-end.

Cochlear mechanics evaluation metrics

The evaluation stimuli were sampled at 20 kHz and had a duration of 102.4 ms (2048 samples) and 128 ms (2560 samples) for the CoNNear and CoNNear-context model, respectively. Stimulus levels were adjusted using the reference pressure of $p_0 = 2 \cdot 10^{-5}$Pa. Only when evaluating how CoNNear generalised to longer duration continuous stimuli (Extended Data Fig.1), or when investigating its real-time capabilities, did we deviate from this procedure. The following sections describe the four cochlear mechanics evaluation

metrics we considered to evaluate the CoNNear predictions. Together, these metrics form a comprehensive description of cochlear processing.

Cochlear filter tuning

A common approach to characterise auditory or cochlear filters is by means of the equivalent-rectangular bandwidth (ERB) or Q_{ERB}. The ERB describes the bandwidth of a rectangular filter which passes the same total power than the filter shape estimated from behavioural or cochlear tuning curve experiments [63], and presents a standardised way to characterise the tuning of the asymmetric auditory/cochlear filter shapes. The ERB is commonly used to describe the frequency and level-dependence of human cochlear filtering [4, 46, 64], and Q_{ERB} to describe level-dependent cochlear filter characteristics from BM impulse response data [19, 65]. We calculated Q_{ERB} as:

$$Q_{ERB} = \frac{CF}{ERB}. \tag{1}$$

The ERB was determined from the power spectrum of a simulated BM time-domain response to an acoustic click stimulus using the following steps [65]: (i) compute the Fast Fourier Transform of the BM displacement at the considered CF, (ii) compute the area underneath the power spectrum, and (iii) divide the area by the CF. The frequency- and level-dependence of CoNNear predicted cochlear filters were compared against TL-model predictions and experimental Q_{ERB} values reported for humans [4].

The acoustic stimuli were condensation clicks of 100-μs duration and were scaled to the desired peak-equivalent sound pressure level (dB peSPL), to yield a peak-to-peak click amplitude that matched that of a pure-tone with the same dB SPL level (L):

$$\text{click}(t) = 2\sqrt{2} \cdot p_0 \cdot 10^{L/20} \cdot x(t) \text{ with } x(t) = \begin{cases} 1 & \text{for } t \leq 100\,\mu s \\ 0 & \text{for } t > 100\,\mu s \end{cases} \tag{2}$$

Cochlear Excitation Patterns

Cochlear excitation patterns can be constructed from the RMS energy of the BM displacement or velocity at each measured CF in response to tonal stimuli of different levels. Cochlear excitation patterns show a characteristic half-octave basal-ward shift of their maxima as stimulus level increases [40]. Cochlear excitation patterns also reflect the level-dependent nonlinear compressive growth of BM-responses when stimulating the cochlea with a pure-tone of the same frequency as the CF of the cochlear measurement site [3]. Cochlear pure-tone transfer-functions and excitation patterns have in several studies been used to describe the level-dependence and tuning properties of cochlear mechanics [2, 3, 40]. We calculated excitation patterns for all 201 simulated BM displacement waveforms in response to pure tones of 0.5, 1 and 2 kHz frequencies and levels between 10 and 90 dB SPL using:

$$\text{tone}(t) = p_0 \cdot \sqrt{2} \cdot 10^{L/20} \cdot \sin(2\pi f_{tone} t), \tag{3}$$

where t corresponds to a time vector of 2048 samples, L to the desired RMS level in dB SPL, and f_{tone} to the stimulus frequencies. The pure-tones were multiplied with a Hanning-shaped 10-ms on- and offset ramp to ensure a gradual onset.

Cochlear Dispersion

Click stimuli can also be used to characterise the cochlear dispersion properties, as their short duration allows for an easy separation of the cochlear response from the evoking stimulus. At the same time, the broad frequency spectrum of the click excites a large portion of the BM. Cochlear dispersion stems from the longitudinal-coupling and tuning properties of BM mechanics [66] and is observed through later click response onsets for BM responses associated with more apical CFs. In humans, the cochlear dispersion delay mounts up to 10-12 ms for stimulus frequencies associated with apical processing [67]. Here, we use clicks of

various sound intensities to evaluate whether CoNNear produced cochlear dispersion and BM click responses in line with predictions from the TL-model.

Distortion-product otoacoustic emissions (DPOAEs)

DPOAEs can be recorded in the ear-canal using a sensitive microphone and are evoked by two pure-tones with frequencies f_1 and f_2 and SPLs of L_1 and L_2, respectively. For pure tones with frequency ratios between 1.1 and 1.3 [68], local nonlinear cochlear interactions generate distortion products, which can be seen in the ear-canal recordings as frequency components which were not originally present in the stimulus. Their strength and shape depends on the properties of the compressive cochlear nonlinearity associated with the electro-mechanical properties of cochlear outer-hair-cells [39], and the most prominent DPOAEs appear at frequencies of $2f_2 - f_1$ and $2f_1 - f_2$. Even though CoNNear was not designed or trained to simulate DPs, they form an excellent evaluation metric, as realistically simulated DPOAE properties would demonstrate that CoNNear was able to capture even the epiphenomena associated with cochlear processing. As a proxy measure for ear-canal recorded DPOAEs, we considered the BM displacement at the highest simulated CF which, in the real ear, would drive the middle-ear and eardrum to yield the ear-canal pressure waveform in an OAE recording. We compared simulated DPs extracted from the fast Fourier transform of the BM displacement response to simultaneously presented pure tones of f_1 and $f_2 = 1.2f_1$ with levels according to the commonly adopted experimental scissors paradigm: $L_1 = 0.4L_2 + 39$ [50]. We considered f_1 frequencies between 1 and 6 kHz and L_2 levels between 10 and 100 dB SPL.

Additional Information

Acknowledgments

Competing interests

A patent application (PCTEP2020065893) was filed by UGent on the basis of the research presented in this manuscript. Inventors on the application are Sarah Verhulst, Deepak Baby, Fotios Drakopoulos and Arthur Van Den Broucke.

Data availability

The source code of the TL-model used for training is available via `10.5281/zenodo.3717431` or `github/HearingTechnology/Verhulstetal2018Model`, the TIMIT speech corpus used for training can be found online [45]. All figures in this paper can be reproduced using the trained CoNNear model.

Code availability

The code for the trained CoNNear model, including instructions of how to execute it is available from github.com/HearingTechnology/CoNNear_cochlea or 10.5281/zenodo.4056552 . A non-commercial, academic UGent license applies.

References

1. von Békésy, G. Travelling Waves as Frequency Analysers in the Cochlea. *Nature* **225**, 1207–1209 (1970).

2. Narayan, S.S., Temchin, A.N., Recio, A. & Ruggero, M.A. Frequency tuning of basilar membrane and auditory nerve fibers in the same cochleae. *Science* **282**, 1882–1884 (1998).

3. Robles, L. & Ruggero, M.A. Mechanics of the mammalian cochlea. *Phys. Rev.* **81**, 1305–1352 (2001).

4. Shera, C.A., Guinan, J.J. & Oxenham, A.J. Revised estimates of human cochlear tuning from otoacoustic and behavioral measurements. *Proc. Nat. Acad. Sci.* **99**, 3318–3323 (2002).

5. Oxenham, A.J. & Shera, C.A. Estimates of human cochlear tuning at low levels using forward and simultaneous masking. *J. Assoc. Res. Otolaryngol.* **4**, 541–554 (2003).

6. Greenwood, D.D. A cochlear frequency-position function for several species—29 years later. *J. Acoust. Soc. Am.* **87**, 2592–2605 (1990).

7. Jepsen, M.L. & Dau, T. Characterizing auditory processing and perception in individual listeners with sensorineural hearing loss. *J. Acoust. Soc. Am.* **129**, 262–281 (2011).

8. Bondy, J., Becker, S., Bruce, I., Trainor, L. & Haykin, S. A novel signal-processing strategy for hearing-aid design: neurocompensation. *Sig. Process.* **84**, 1239–1253 (2004).

9. Ewert, S.D., Kortlang, S. & Hohmann, V. A Model-based hearing aid: Psychoacoustics, models and algorithms. *Proc. Meetings on Acoust.* **19**, 050187 (2013).

10. Mondol, S. & Lee, S. A machine learning approach to fitting prescription for hearing aids. *Electronics* **8**, 736 (2019).

11. Lyon, R.F. *Human and Machine Hearing: Extracting Meaning from Sound* (Cambridge University Press, 2017).

12. Baby, D. & Van hamme, H. Investigating modulation spectrogram features for deep neural network-basedautomatic speech recognition. In *Proc. Insterspeech*, 2479–2483 (Dresden, Germany, 2015).

13. de Boer, E. Auditory physics. physical principles in hearing theory. i. *Phys. Rep.* **62**, 87–174 (1980).

14. Diependaal, R.J., Duifhuis, H., Hoogstraten, H.W. & Viergever, M.A. Numerical methods for solving one-dimensional cochlear models in the time domain. *J. Acoust. Soc. Am.* **82**, 1655–1666 (1987).

15. Zweig, G. Finding the impedance of the organ of corti. *J. Acoust. Soc. Am.* **89**, 1229–1254 (1991).

16. Talmadge, C.L., Tubis, A., Wit, H.P. & Long, G.R. Are spontaneous otoacoustic emissions generated by self-sustained cochlear oscillators? *J. Acoust. Soc. Am.* **89**, 2391–2399 (1991).

17. Moleti, A. *et al.* Transient evoked otoacoustic emission latency and estimates of cochlear tuning in preterm neonates. *J. Acoust. Soc. Am.* **124**, 2984–2994 (2008).

18. Epp, B., Verhey, J.L. & Mauermann, M. Modeling cochlear dynamics: Interrelation between cochlea mechanics and psychoacoustics. *J. Acoust. Soc. Am.* **128**, 1870–1883 (2010).

19. Verhulst, S., Dau, T. & Shera, C.A. Nonlinear time-domain cochlear model for transient stimulation and human otoacoustic emission. *J. Acoust. Soc. Am.* **132**, 3842–3848 (2012).

20. Zweig, G. Nonlinear cochlear mechanics. *J. Acoust. Soc. Am.* **139**, 2561–2578 (2016).

21. Hohmann, V. *Signal Processing in Hearing Aids*, 205–212 (Springer New York, New York, NY, 2008).

22. Rascon, C. & Meza, I. Localization of sound sources in robotics: A review. *Robot. Auton. Syst.* **96**, 184–210 (2017).

23. Mogran, N., Bourlard, H. & Hermansky, H. *Automatic Speech Recognition: An Auditory Perspective*, 309–338 (Springer New York, New York, NY, 2004).

24. Patterson, R.D., Allerhand, M.H. & Giguère, C. Time-domain modeling of peripheral auditory processing: A modular architecture and a software platform. *J. Acoust. Soc. Am.* **98**, 1890–1894 (1995).

25. Shera, C.A. Frequency glides in click responses of the basilar membrane and auditory nerve: Their scaling behavior and origin in traveling-wave dispersion. *J. Acoust. Soc. Am.* **109**, 2023–2034 (2001).

26. Shera, C.A. & Guinan, J.J. Mechanisms of mammalian otoacoustic emission. In *Active Processes and Otoacoustic Emissions in Hearing*, 305–342 (Springer, 2008).

27. Hohmann, V. Frequency analysis and synthesis using a Gammatone filterbank. *Acta Acust. United Ac.* **88**, 433–442 (2002).

28. Saremi, A. *et al.* A comparative study of seven human cochlear filter models. *J. Acoust. Soc. Am.* **140**, 1618–1634 (2016).

29. Lopez-Poveda, E.A. & Meddis, R. A human nonlinear cochlear filterbank. *J. Acoust. Soc. Am.* **110**, 3107–3118 (2001).

30. Lyon, R.F. Cascades of two-pole–two-zero asymmetric resonators are good models of peripheral auditory function. *J. Acoust. Soc. Am.* **130**, 3893–3904 (2011).

31. Saremi, A. & Lyon, R.F. Quadratic distortion in a nonlinear cascade model of the human cochlea. *J. Acoust. Soc. Am.* **143**, EL418–EL424 (2018).

32. Altoè, A., Charaziak, K.K. & Shera, C.A. Dynamics of cochlear nonlinearity: Automatic gain control or instantaneous damping? *J. Acoust. Soc. Am.* **142**, 3510–3519 (2017).

33. Baby, D. & Verhulst, S. SERGAN: Speech enhancement using relativistic generative adversarial networks with gradient penalty. In ”*Acoustics, Speech and Signal Processing (ICASSP), IEEE Int. Conf.*, 106–110 (Brighton, UK, 2019).

34. Pascual, S., Bonafonte, A. & Serrà, J. SEGAN: speech enhancement generative adversarial network. In *Interspeech*, 3642–3646 (ISCA, 2017).

35. Drakopoulos, F., Baby, D. & Verhulst, S. Real-Time Audio Processing on a Raspberry Pi using Deep Neural Networks. In *23rd Int. Congress on Acoustics (ICA)* (Aachen, Germany, 2019).

36. Altoè, A., Pulkki, V. & Verhulst, S. Transmission line cochlear models: Improved accuracy and efficiency. *J. Acoust. Soc. Am.* **136**, EL302–EL308 (2014).

37. Verhulst, S., Altoè, A. & Vasilkov, V. Computational modeling of the human auditory periphery: Auditory-nerve responses, evoked potentials and hearing loss. *Hear. Res.* **360**, 55–75 (2018).

38. Oxenham, A.J. & Wojtczak, M. *Frequency selectivity and masking: Perception* (Oxford University Press, 2010).

39. Robles, L., Ruggero, M.A. & Rich, N.C. Two-tone distortion in the basilar membrane of the cochlea. *Nature* **349**, 413 (1991).

40. Ren, T. Longitudinal pattern of basilar membrane vibration in the sensitive cochlea. *Proc. Nat. Acad. Sci.* **99**, 17101–17106 (2002).

41. Precise and full-range determination of two-dimensional equal loudness contours. Standard, International Organization for Standardization, Geneva, CH (2003).

42. Lorenzi, C., Gilbert, G., Carn, H., Garnier, S. & Moore, B.C. Speech perception problems of the hearing impaired reflect inability to use temporal fine structure. *Proc. Nat. Acad. Sci.* **103**, 18866–18869 (2006).

43. Isola, P., Zhu, J.Y., Zhou, T. & Efros, A.A. Image-to-image translation with conditional adversarial networks. In *IEEE-CVPR*, 5967–5976 (2017).

44. LeCun, Y., Bengio, Y. & Hinton, G. Deep learning. *Nature* **521**, 436–444 (2015).

45. Garofolo, J.S. *et al.* Darpa timit acoustic phonetic continuous speech corpus cdrom (1993).

46. Shera, C.A., Guinan, J.J. & Oxenham, A.J. Otoacoustic estimation of cochlear tuning: validation in the chinchilla. *J. Assoc. Res. Otolaryngol.* **11**, 343–365 (2010).

47. Russell, I., Cody, A. & Richardson, G. The responses of inner and outer hair cells in the basal turn of the guinea-pig cochlea and in the mouse cochlea grown in vitro. *Hear. Res.* **22**, 199–216 (1986).

48. Houben, R. *et al.* Development of a dutch matrix sentence test to assess speech intelligibility in noise. *Int. J. Audiol.* **53**, 760–763 (2014).

49. Paul, D.B. & Baker, J.M. The design for the wall street journal-based CSR corpus. In *The Second International Conference on Spoken Language Processing, ICSLP* (ISCA, 1992).

50. Kummer, P., Janssen, T., Hulin, P. & Arnold, W. Optimal L1−L2 primary tone level separation remains independent of test frequency in humans. *Hear. Res.* **146**, 47–56 (2000).

51. Dorn, P.A. *et al.* Distortion product otoacoustic emission input/output functions in normal-hearing and hearing-impaired human ears. *J. Acoust. Soc. Am.* **110**, 3119–3131 (2001).

52. Janssen, T. & Müller, J. Otoacoustic emissions as a diagnostic tool in a clinical context. In *Active Processes and Otoacoustic Emissions in Hearing*, 421–460 (Springer, 2008).

53. Verhulst, S., Ernst, F., Garrett, M. & Vasilkov, V. Suprathreshold psychoacoustics and envelope-following response relations: Normal-hearing, synaptopathy and cochlear gain loss. *Acta Acus. united Ac.* **104**, 800–803 (2018).

54. Verhulst, S., Bharadwaj, H.M., Mehraei, G., Shera, C.A. & Shinn-Cunningham, B.G. Functional modeling of the human auditory brainstem response to broadband stimulation. *J. Acoust. Soc. Am.* **138**, 1637–1659 (2015).

55. Kell, A.J., Yamins, D.L., Shook, E.N., Norman-Haignere, S.V. & McDermott, J.H. A task-optimized neural network replicates human auditory behavior, predicts brain responses, and reveals a cortical processing hierarchy. *Neuron* **98**, 630–644 (2018).

56. Akbari, H., Khalighinejad, B., Herrero, J.L., Mehta, A.D. & Mesgarani, N. Towards reconstructing intelligible speech from the human auditory cortex. *Sci. Rep.* **9**, 1–12 (2019).

57. Kell, A.J. & McDermott, J.H. Deep neural network models of sensory systems: windows onto the role of task constraints. *Curr. Opin. Neurobiolog.* **55**, 121–132 (2019).

58. Amsalem, O. *et al.* An efficient analytical reduction of detailed nonlinear neuron models. *Nat. Comm.* **11**, 1–13 (2020).

59. Richards, B.A. *et al.* A deep learning framework for neuroscience. *Nature Neurosci.* **22**, 1761–1770 (2019).

60. Kingma, D.P. & Ba, J. Adam: A method for stochastic optimization. *CoRR* **abs/1412.6980** (2014). `1412.6980`.

61. Chollet, F. *et al.* Keras. https://keras.io (2015).

62. Abadi, M. *et al.* TensorFlow: Large-scale machine learning on heterogeneous systems. https://www.tensorflow.org/ (2015). Software available from tensorflow.org.

63. Moore, B.C. & Glasberg, B.R. Suggested formulae for calculating auditory-filter bandwidths and excitation patterns. *J. Acoust. Soc. Am.* **74**, 750–753 (1983).

64. Glasberg, B.R. & Moore, B.C. Derivation of auditory filter shapes from notched-noise data. *Hear. Res.* **47**, 103–138 (1990).

65. Raufer, S. & Verhulst, S. Otoacoustic emission estimates of human basilar membrane impulse response duration and cochlear filter tuning. *Hear. Res.* **342**, 150–160 (2016).

66. Ramamoorthy, S., Zha, D.J. & Nuttall, A.L. The biophysical origin of traveling-wave dispersion in the cochlea. *Biophys. J.* **99**, 1687–1695 (2010).

67. Dau, T., Wegner, O., Mellert, V. & Kollmeier, B. Auditory brainstem responses with optimized chirp signals compensating basilar-membrane dispersion. *J. Acoust. Soc. Am.* **107**, 1530–1540 (2000).

68. Neely, S.T., Johnson, T.A., Kopun, J., Dierking, D.M. & Gorga, M.P. Distortion-product otoacoustic emission input/output characteristics in normal-hearing and hearing-impaired human ears. *J. Acoust. Soc. Am.* **126**, 728–738 (2009).

1   Extended Data

**Extended Data Table 1: Overview of the CoNNear architecture parameters.**

Fixed parameters	Summary
Window length	The model input size (L) was 2048 samples ($\approx$ 100 ms) for the CoNNear model and $2048 + 2 \cdot 256 = 2560$ samples for the CoNNear-context model. These input sizes were adopted for all training procedures and evaluation metrics, but do not preclude the use of other input durations for the trained CoNNear model. The generalisability of CoNNear towards longer duration stimuli was evaluated using inputs of 10048 and 16384 samples, while its real-time capabilities were evaluated using inputs of 1048 samples.
CNN parameters	The filters in the encoder layers use a stride of 2 for dimensionality reduction, and were upscaled by a factor of 2 in the decoder layers. All CNN layers had a fixed filter length of 64 samples, using 128 filters per layer except for the last decoder layer which had N_{CF} filters to match the BM vibration outputs of the reference TL-model.
Number of cochlear output channels	CoNNear was trained to generate BM displacements of 201 cochlear filters with CFs between 100 Hz and 12 kHz according to the Greenwood map [6].
Hyperparameters	**Summary**
Number of layers	Increasing the number of layers increases the representational capacity of the model, but evidently also increases the computational complexity (see also Extended Data Table 2). We investigated CoNNear architectures with layer depths of 4, 6 and 8 to determine the minimum required model size that reliably captured the desired cochlear mechanical properties.
Activation function	The shape of the activation function, or nonlinearity, between the CNN layers is crucial to enable CoNNear to learn the cochlear compression properties associated with the role of the cochlear outer hair cells (OHCs). To mimic the original shape of the OHC input/output function [47], the activation function should cross the x-axis. Standard activation functions (e.g., sigmoid, ReLUs) do not cross the x-axis, and may end up limiting the CoNNear model from learning realistic level-dependent BM impulse response properties. We hence compare the performance of architectures with activation functions that crossed the x-axis, i.e., the parametric rectified linear unit (PReLU) and hyperbolic-tangent (tanh) nonlinearities.
Context	Adding context information to CoNNear can help to avoid discontinuities near the boundaries of the simulated L-sized windows. We examined whether adding a context window of $L_l = L_r = 256$ samples would increase the quality of the CoNNear model predictions.

Extended Data Table 2: Activation function comparison. The first column details the CoNNear architecture. The next columns describe the total number of required model parameters, the required training time per epoch of 2310 TIMIT training sentences and average L1 loss across all windows of the TIMIT training set. Average L1 losses were also computed for BM displacement predictions to a number of unseen acoustic stimuli (click and 1-kHz pure tones) with levels between 0 and 90 dB SPL. Lastly, average L1 loss was also computed for the 550 sentences of the TIMIT test set. For each evaluated category, the best performing architecture is highlighted in bold font.

Model	#Param	Time/Epoch [h]	Training set	Click	1kHz	Test set
			Average L1 loss			
PReLU/8 lay./no context	11,982,464	1.89	0.0267	0.0126	0.0302	0.0312
tanh/8 lay./no context	11,507,328	**1.84**	0.0123	0.0023	0.0116	0.0124
tanh/8 lay./context	11,689,984	2.18	**0.0087**	**0.0017**	**0.0107**	**0.0081**

Extended Data Table 3: CNN layer depth comparison. The first column details the CoNNear architecture. The next columns describe the total number of required model parameters, the required training time per epoch of 2310 TIMIT training sentences and average L1 loss across all windows of the TIMIT training set. Average L1 losses were also computed for BM displacement predictions to a number of unseen acoustic stimuli (click and 1-kHz pure tones) with levels between 0 and 90 dB SPL. Lastly, average L1 loss was also computed for the 550 sentences of the TIMIT test set. For each evaluated category, the best performing architecture is highlighted in bold font.

|				Average L1 loss			
Model	#Param	Time/Epoch [h]	Training set	Click	1kHz	Test set
tanh/4 lay./context	5,398,528	**2.13**	0.0187	0.0035	0.0171	0.0190
tanh/6 lay./context	8,544,256	2.15	0.0102	0.0022	0.0123	0.0105
tanh/8 lay./context	11,689,984	2.18	**0.0087**	**0.0017**	**0.0107**	**0.0081**
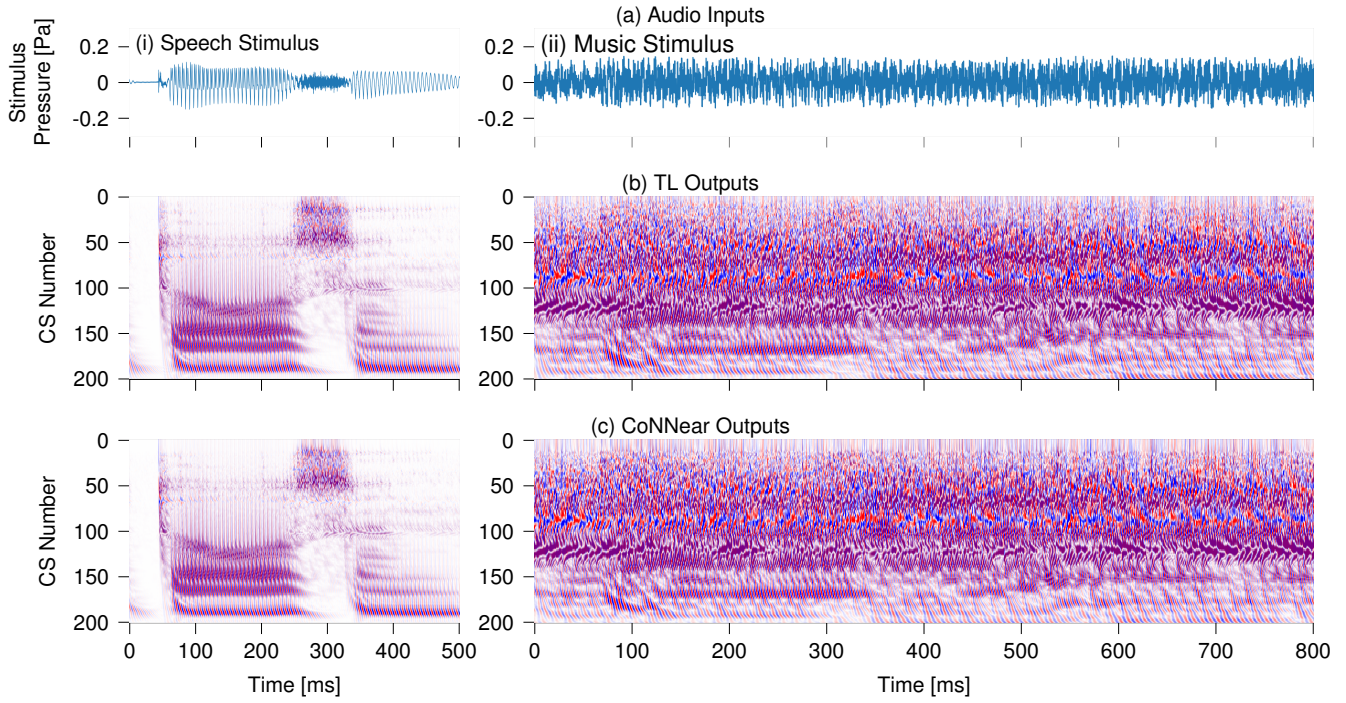
Extended Data Fig.1: Simulated BM displacements for a 10048-sample speech stimulus and a 16384-sample music stimulus. The stimulus waveform is depicted in panel (a) and panels (b)-(c) depict instantaneous BM displacement intensities (darker colours = higher intensities) of the simulated TL-model (b) and CoNNear (c) outputs. The $N_{CF}=201$ considered output channels are labelled per channel number: channel 1 corresponds to a CF of 12 kHz and channel 201 to a CF of 100 Hz. The same colour scale was used for both simulations and ranged between -0.5 μm (blue) and 0.5 μm (red). The left panels show simulations to a speech stimulus from the Dutch matrix test [48] and the right panels shows simulations to a music fragment (Interpol - Evil).
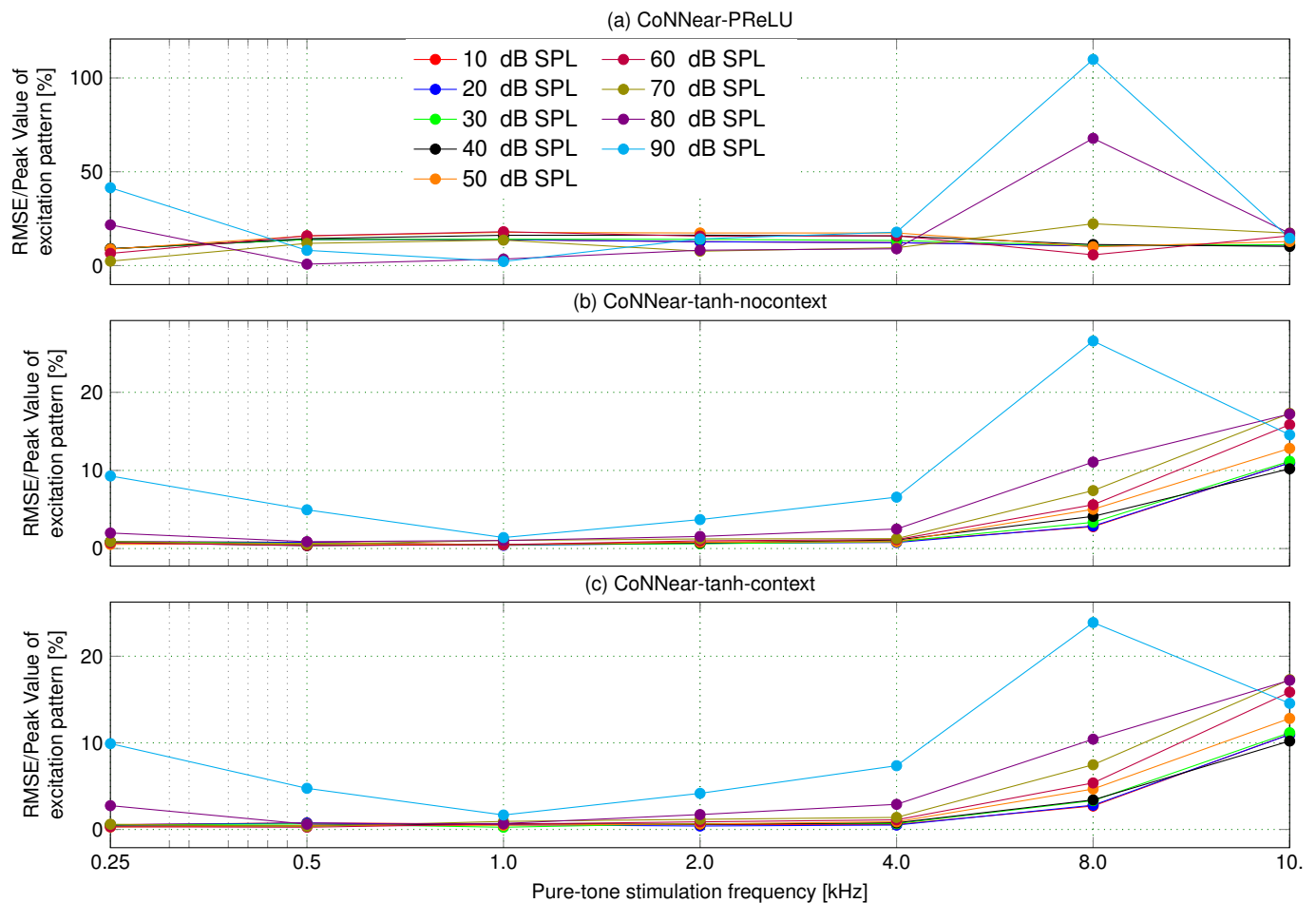
Extended Data Fig.2: Root mean-square error (RMSE) between simulated excitation patterns of the TL and CoNNear models reported as fraction of the TL excitation pattern maximum (cf. Fig. 3). Using the PReLU activation function (a) leads to an overall high RMSE as this architecture failed to learn the level-dependent cochlear compression characteristics and filter shapes. The models using the tanh nonlinearity (b),(c) did learn to capture the level-dependent properties of cochlear excitation patterns, and performed with errors below 5% for the frequency ranges and stimulus levels captured by the speech training data (for CFs below 5 kHz, and stimulation levels below 90 dB SPL) The RMSE increased above 5% for all architectures when evaluating its performance on 8- and 10-kHz excitation patterns. This decreased performance results from the limited frequency content of the TIMIT training material.
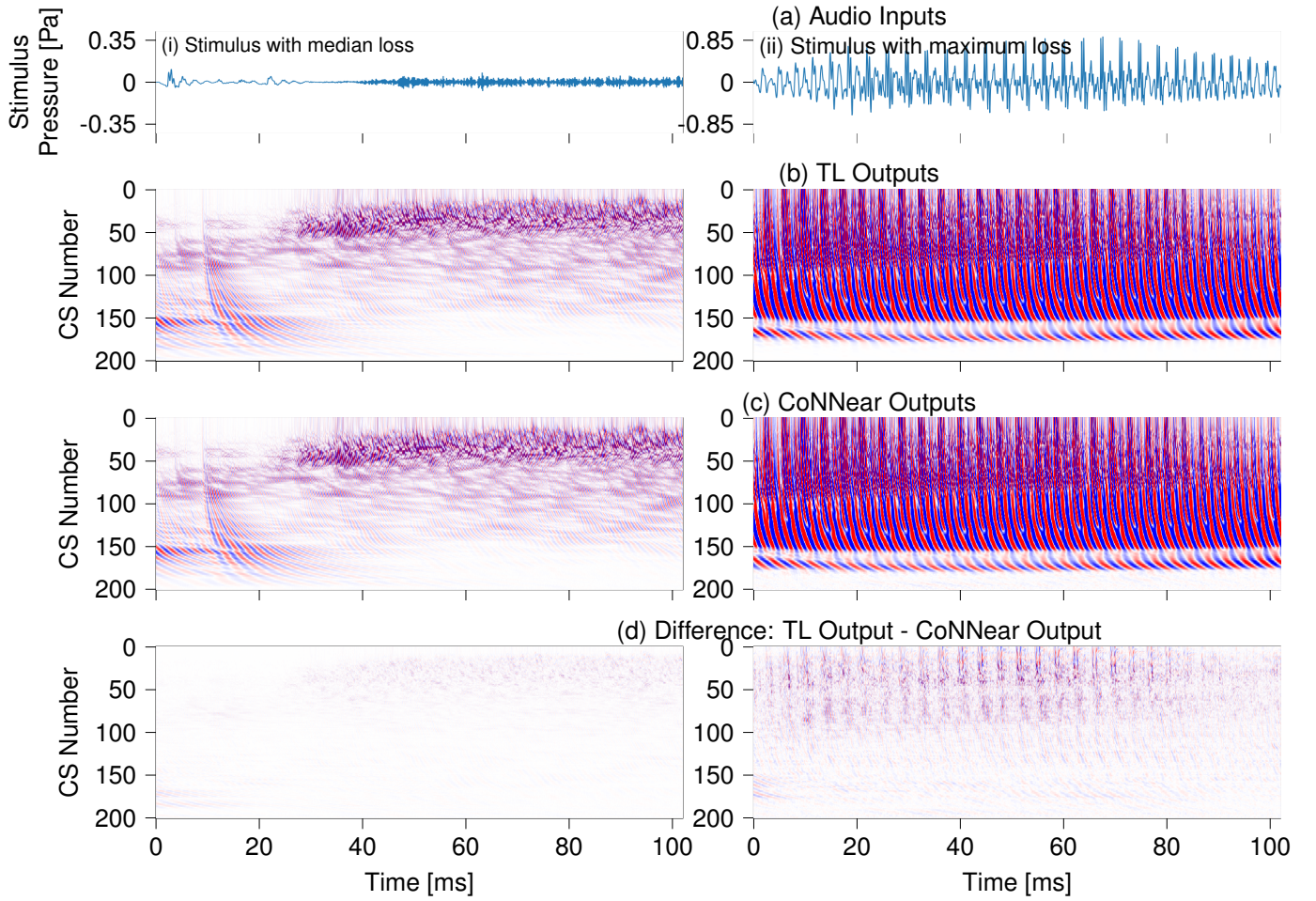
Extended Data Fig.3: Comparing TL and CoNNear model predictions at the median and maximum L1 prediction error. The figure visually compares BM displacement intensities of the BM (b) and CoNNear (c) model to audio fragments which resulted in the median and maximum L1 errors of 0.008 and 0.038 simulated for the TIMIT test set (Fig. 5). The $N_{CF}=201$ considered output channels are labelled per channel number: channel 1 corresponds to a CF of 12 kHz and channel 201 to a CF of 100 Hz. The same colour scale was used for both simulations and ranged between -0.5 μm (blue) and 0.5 μm (red).